

Black Hole Growth from Cosmological N-body Simulations

Miroslav Micic^{1*}, Kelly Holley-Bockelmann¹, Steinn Sigurdsson²

¹ *Department of Physics & Astronomy, Vanderbilt University*

² *Department of Astronomy & Astrophysics, Pennsylvania State University*

24 October 2018

ABSTRACT

We use high resolution cosmological N-body simulations to study the growth of intermediate to supermassive black holes (SMBH) from redshift 49 to zero. Our cosmological volume and mass resolution is small enough that we can track the growth of black holes from the seeds of population III stars to black holes in the range of $10^3 < M < 10^7$ solar mass black holes – not quasars, but rather intermediate mass black holes to low-mass SMBHs. These lower mass black holes are the primary observable for the Laser Interferometer Space Antenna (LISA), and may remain the most common black hole in the universe. The large-scale dynamics of the black holes are followed accurately within the simulation down to scales of 1 kpc; thereafter, we follow the merger analytically from the last dynamical friction phase to black hole coalescence. We find that the merger rate of these black holes is $R \sim 25 \text{ yr}^{-1}$ between $8 \leq z \leq 11$ and $R = 10 \text{ yr}^{-1}$ at $z=3$. Before the merger occurs the incoming IMBH may be observed with a next generation of X-ray telescopes as a ULX source with a rate of about $\sim 3 - 7 \text{ yr}^{-1}$ for $1 \leq z \leq 5$. When we include the lowest predicted efficiency of Pop III star formation, the black hole merger rate decreases to $R \sim 2 - 3 \text{ yr}^{-1}$ which is still a reliable LISA source.

We develop an analytic prescription that captures the most important black hole growth mechanisms: galaxy merger-driven gas accretion and black hole coalescence. This prescription is based on sophisticated gas-rich galaxy merger simulations that include feedback and star formation. Using this simple prescription, we find that we can grow an analogue of the Milky Way black hole and dark matter halo by redshift zero. In our volume, this supermassive black hole was in place with most of its mass by $z = 4.7$, and most of the growth was driven by gas accretion excited by major mergers.

Hundreds of black holes have failed to coalesce with the SMBH by $z = 0$, some with masses of $10^4 M_\odot$. As these black holes orbit within the dark matter halo, they may have luminosities up to $\sim 30000 L_\odot$ if the halo is suffused with tenuous hot gas. These bright X-ray sources can easily be observed with Chandra at distances of ~ 100 kpc.

Key words:

galaxies, intermediate mass black holes, supermassive black holes, gravitational waves, dark matter halos, n-body simulations

1 INTRODUCTION

Supermassive black holes, with masses of $10^6 M_\odot \leq M \leq 10^{10} M_\odot$ are widely believed to dwell at the centers of elliptical galaxies and spiral bulges (e.g. Kormendy & Richstone 1995), and the most massive of these black holes are tied to quasar

* E-mail: m.micic@vanderbilt.edu, k.holley@vanderbilt.edu, steinn@astro.psu.edu

phenomena at high redshift (Greenstein & Matthews 1963). There is abundant evidence that when a SMBH is in place, it transforms the structure and evolution of the galaxy, from powering active galactic nuclei at high redshifts (Rees 1984, Alexander et al. 2005, Fan 2005), to regulating star formation throughout the galaxy (Di Matteo et al. 2005, Cox et al. 2008), to scouring the galactic nucleus of stars during SMBH mergers (Ebisuzaki et al. 1991, Quinlan 1996, Makino 1997, Milosavljevic & Merritt 2001, Volonteri et al. 2003).

This deep connection between the evolution of SMBHs and galaxies is perhaps best encapsulated in a remarkable correlation between the SMBH mass and the velocity dispersion of the host spheroid (Gebhardt et al. 2000, Ferrarese & Merritt 2000, Tremaine et al. 2002). This $M_{\text{BH}} - \sigma$ correlation appears to be intrinsically perfect, at least for a sample of nearby bright spiral and elliptical galaxies with clear dynamical SMBH signatures. There is even a suggestion that the $M_{\text{BH}} - \sigma$ relation may hold for black holes on a much smaller mass scale of $10^3 < M_{\text{BH}} < 10^5 M_{\odot}$ – the intermediate mass black holes, or IMBHs (Filippenko & Ho 2003, Barth et al. 2004, Gebhardt et al. 2005, Green & Ho 2004).

In searching for the root cause of this galaxy-SMBH connection, a handful of SMBH mass-‘host property’ correlations have emerged. Many of these correlations, admittedly, can simply be byproducts of the $M_{\text{BH}} - \sigma$ relation, since the velocity dispersion of a galaxy is a measure of its underlying potential. However, several observational and theoretical studies have linked the SMBH mass with the mass of the host dark matter halo (Ferrarese 2002, Baes et al. 2003, Shankar et al. 2006). This relation is a boon to theorists because many of the leading explanations of SMBH birth and growth are driven by hierarchical structure formation (Hopkins et al. 2005, Wythe & Loeb 2005, Granato et al. 2001, Menou et al. 2001, Adams et al. 2001, Monaco et al. 2000, Silk & Rees 1998, Haehnelt et al. 1998, Haehnelt & Kauffmann 2000, Cattaneo et al. 1999, Loeb & Rasio 1994), and are therefore tied to the mass of the dark matter halo.

In the current picture of SMBH assembly, the black hole begins life as a low mass “seed” black hole at high redshift. It’s not clear, though, when exactly these BH seeds emerge or what mass they have at birth. SMBH seeds may have been spawned from the accretion of low angular momentum gas in a dark matter halo (Koushiappas et al. 2004, Bromm & Loeb 2003), the coalescence of many seed black holes within a halo (Begelman & Rees 1978, Islam et al. 2004), or from an IMBH formed, perhaps, by runaway stellar collisions (Portegies Zwart et al. 2004, Miller & Colbert 2004, van der Marel 2004). However, the most likely candidates for SMBH seeds are the remnants that form from the first generation of stars sitting deep within dark matter halos (Madau & Rees 2001, Heger et al. 2003, Volonteri et al. 2003, Islam et al. 2003, Wise & Abel 2005) – so called Population III stars. With masses $< 10^3 M_{\odot}$, these relic seeds are predicted to lie near the centers of dark matter halos between $z \sim 12 - 20$ (Bromm et al. 1999, Abel et al. 2000, 2002). Structure formation dictates that dark matter halos form in the early universe and hierarchically merge into larger bound objects, so naturally as dark matter halos merge, seed black holes sink to the center through dynamical friction and eventually coalesce. Dark matter halo mergers become synonymous, then, with black hole mergers at these masses and redshifts. This means that although the seed formation stops at $z \sim 12$ as Population III supernovae rates drop to zero (Wise & Abel 2005), SMBH growth continues as dark matter halo mergers proceed to low redshifts.

Gas accretion is thought to play a critical role in fueling the early stages of black hole growth (David et al. 1987, Kauffmann & Haehnelt 2000, Merloni 2004), and this may explain the tightness of the $M_{\text{BH}} - \sigma$ relation (Burkert & Silk 2001, Haehnelt & Kauffmann 2000, Di Matteo et al. 2005, Kazantzidis et al. 2005, Robertson et al. 2006). Since high redshift galaxies are thought to be especially gas-rich, each merger brings a fresh supply of gas to the center of the galaxy, and new fuel to the growing supermassive black hole (Mihos & Hernquist 1994, Di Matteo et al. 2003). From a combination of gas accretion and binary black hole coalescence, it is thought that these Pop III-generated seeds may form the SMBHs we observe today (Soltan 1982, Schneider et al. 2002).

During a galaxy merger, each black hole sinks to the center of the new galaxy potential due to dynamical friction and eventually becomes bound as a binary (Kazantzidis et al. 2005; Escala et al. 2005). Dynamical friction then continues to shrink the orbit until the binary is hard (i.e, the separation between each black hole, a_{BBH} , is such that the system tends to lose energy during stellar encounters) (Heggie et al. 2007). Thereafter, further decay is mediated by 3-body scattering with the ambient stellar background until the binary becomes so close that the orbit can lose energy via gravitational radiation. In studies of static, spherical potentials, it may be difficult for stellar encounters alone to cause the binary to transition between the 3-body scattering phase and the gravitational radiation regime (Milosavljevic & Merritt 2003). However, in gas-rich or non-spherical systems, the binary rapidly hardens and coalesces into one black hole, emitting copious gravitational radiation in the process (Mayer et al. 2007, Kazantzidis et al. 2005, Berczik et al. 2006; Sigurdsson 2003; Holley-Bockelmann & Sigurdsson 2006).

In our previous work, we calculated the cosmological merger rate for black holes between $200 - 3 \times 10^7 M_{\odot}$ from redshift 20-0 (Micic et al. 2007). Our approach combined high-resolution, small-volume cosmological N-body simulations with analytic prescriptions for the dynamics of merging black holes below our resolution limit; this allowed us to explore different black hole growth mechanisms and seed formation scenarios while also accurately simulating the rich and varied merger history of the host dark matter halos. However, our original work treated the black hole merger timescales rather optimistically; the black holes were said to merge immediately after the dark matter halos merge. In addition, we assumed that black hole seed

formation is prolific, occurring in every dark matter halo capable of hosting a Population III star. The merger rates from Micic et al. 2007, then, may be considered upper limits for a given black hole growth scenario.

It is expected that only a fraction of first stars collapse into massive black holes. Calculating this fraction would be trivial if the POP III initial mass function is known. Unfortunately, the initial mass function of the first stars is still very uncertain, mostly because the primordial fragmentation process is still very poorly understood (Nakamura & Umemura 2001; Omukai & Yoshii 2003). If the initial mass function for the first stars were top heavy (Schneider et al. 2002), $\sim 6\%$ of the total mass in first stars would go into black holes after supernovae collapse. Since half of the mass of each individual first star is ejected during a supernovae (Heger & Woosley 2002), $\sim 12\%$ of first stars produce a black hole. Hence, the fraction of the first stars that produce massive black holes could be as low as 10% , $f_{\text{POPIII}} = 0.1$ (Schneider et al. 2002). This will have a direct consequence on the occupation fraction of halos with seed black holes at high redshift.

Unless the black hole binaries stall at the final parsec, the longest timescale governing the coalescence of two black holes occurs when the host galaxies themselves are still merging. Here, the dynamical evolution of two merging galaxies is driven by the combined effect of dynamical friction that brings the less massive galaxy (satellite) to the center of the larger halo (primary), and the tidal interaction that strips mass from the satellite (e.g. Richstone 1976, Aguilar & White 1986, Holley-Bockelmann & Richstone 1999, Taffoni et al. 2003) and further delays the merger. If the dynamical friction timescale is longer than a Hubble time, the black holes carried by their host galaxies will not be brought close enough to form a binary. This delay in the merger timescale can certainly reduce black hole merger rates.

In this paper, we continue to use this hybrid method to study how our predictions of black hole assembly changes when the effects of black hole seed formation efficiency and dynamical friction are introduced, and what effect these processes have on merger rates. We track the assembly of black holes over a large range of final masses – from seed black holes to SMBHs – over widely varying dynamical histories. We also expand on a prescription to model the growth of the black hole from a seed to a supermassive black hole as a function of the merger history; this prescription is physically motivated by simulations of star formation and feedback, captures the two most important mechanisms by which supermassive black holes assemble, and is very easy to implement in cosmological dark matter-only simulations. With this improved treatment of black hole dynamics and accretion, we derive merger rates of dark matter halos and black holes as a function of mass ratio and redshift. These will be important observables for the Laser Interferometric Space Antenna (LISA), a planned space mission to detect gravitational waves, set to launch in the next decade.

We describe our method in section 2 and introduce the black hole growth prescription. In section 3, we present the results for both the growth of SMBH in our volume and for the properties of rogue black holes; this section includes black hole merger rates, dark matter halo merger rates in this low mass regime, and our derived black hole-host halo relation on this low mass end. We discuss the implications of our results and future work in section 4.

2 METHOD

In this section, we give an overview for how we simulate our small cosmological volume, construct the dark matter halo merger trees, and model the black hole physics.

2.1 Simulation Setup and Dark Matter Halo Merger Tree

Using GADGET (Springel et al. 2001), we performed a high-resolution cosmological N-body simulation within a comoving 10 Mpc^3 section of a Λ CDM universe ($\Omega_{\text{M}}=0.3$, $\Omega_{\Lambda}=0.7$, $\sigma_8=0.9$ and $h=0.7$) from $z = 40$ to $z = 0$. We are using WMAP1 (Bennett et al. 2003) cosmological parameters in this study to compare with our previous work; however, at the time of this paper’s submission, simulations of several small volumes are underway with WMAP3 parameters (Spergel et al. 2007). A detailed description of this simulation can be found in Micic et al. 2006. Briefly, however, we identify high density region within a low-resolution cosmological volume that at $z = 0$ hosts a dark matter halo comparable in size to the halo hosting the Milky Way Galaxy. We then refine a sphere of 2 Mpc around the halo of interest to simulate at a higher resolution with 4.9×10^6 high-resolution particles (softening length 2 kpc comoving). The rest of the box has 2.0×10^6 low-resolution particles (softening length 4 kpc comoving). The mass of each high resolution particle in this simulation is $8.85 \times 10^5 M_{\odot}$, and the mass of each low-resolution particle is $5.66 \times 10^7 M_{\odot}$. In the post-simulation analysis, we identify dark matter structures, seed them with Population III black holes, and follow their merger history from redshift 20 to 0 by constructing numerical merger trees. The method we use is described in detail in Micic et al. 2007.

In our hybrid method, we combine dark matter halo merger trees obtained in numerical simulations with an analytical treatment of the physical processes that arise in the dynamics of galaxy and black hole mergers. Our N-body approach starts with the creation of the halo merger tree. To define the structure of each dark matter halo within the n-body generated merger tree, we assume a Navarro, Frenk, & White (hereafter, NFW) density profile (Navarro, Frenk & White 1995). We set the parameters of a given NFW halo using the approach presented in Bullock et al. 2001, assuming the typical virial mass of a

dark matter halo to be $M_{\text{typ}} = 1.5 \times 10^{13} M_{\odot}$ at redshift 0 and that this mass varies with redshift as: $M_{\text{typ}}(z) = M_{\text{typ}}(z=0) / (1+z)$. The concentration, then, is defined as $c_{\text{vir}} = 9 \mu^{\alpha}$, where μ is the halo mass in units of the typical halo mass at the same redshift, $\mu = M_{\text{halo}}/M_{\text{typ}}$, $\alpha = -0.13$ for $\mu \geq 0.2$ and $\alpha = -0.3$ for $\mu \leq 0.2$. Concentration parameters for all dark matter halos in our merger tree as a function of halo mass are presented in figure 1. For each merger, we tag the more massive halo as the primary, with mass M_p , and the less massive halo as the secondary or satellite halo with mass M_s . Note that the properties of dark matter halos in the mass range of our simulation ($10^{6.5} M_{\odot} \leq M \leq 10^{12} M_{\odot}$) have not been studied at high redshift ($z \geq 3$).

2.2 Black Hole Seed Formation

In the current picture of the evolution of very low metallicity stars, those with an initial mass $30 M_{\odot} \leq M_{\text{POPIII}} \leq 140 M_{\odot}$ and $M_{\text{POPIII}} \geq 260 M_{\odot}$ collapse directly into a black hole (Heger & Woosley 2002). Due to copious mass loss from winds, stars $30 \leq M_{\text{POPIII}}$ form a neutron star or white dwarf, and stars with $140 M_{\odot} \leq M_{\text{POPIII}} \leq 260 M_{\odot}$ go through pair instability supernovae leaving no remnant behind. The initial mass function (IMF) of these first stars is unclear, though, in part due to a lack of understanding of how primordial molecular hydrogen gas clouds fragment. It is expected that the IMF may be top heavy. This is because the accretion rate onto the first stars is large (Omukai & Nishi 1998, Ripamonti et al. 2002) and since dust grains are absent in primordial H_2 gas clouds, the radiative feedback from the forming star is not strong enough to halt further gas accretion (Omukai & Palla 2003, Bromm & Loeb 2004). The latest constraint of the first star's maximum mass comes from modeling the structure of the accretion flow and the evolution of protostars, and sets the maximum mass to $\sim 300 M_{\odot}$. It is unlikely that the Pop III IMF is anything like a Salpeter IMF (power law with -2.35 slope), a canonical IMF used to model metal-enriched stellar populations.

The fraction of the first stars that produce massive black holes could be as low as 10 %, $f_{\text{POPIII}} = 0.1$ (Schneider et al. 2002). We do note that 10% is a lower constraint and that much higher efficiency would not be unexpected. Since the formation of the first stars is only limited, theoretically, by the minimum mass of the host dark matter halo (Wise & Abel 2005), there is no expected correlation between the masses of first stars and the masses of their host halos. We choose our seed black hole mass to be $200 M_{\odot}$ in this work. In 100 realizations, we randomly select 10% of dark matter halos that can host seed black holes and remove the rest of the seeds from our merger tree. The effect of the initial occupation fraction on the black hole merger rates is direct and dramatic, as can be seen in figure 3.

2.3 Dynamical Friction

There are two important mechanisms that lead to the formation of a massive black hole binary at the center of a galaxy. First, dynamical friction expedites the merger of two dark matter halos and later the merger of the galaxies they host. In this manner, merging galaxies can efficiently shepherd massive black holes to the center of the new system, roughly to the inner kiloparsec (see Colpi et al. 2007 for a review). Second, dynamical friction from the gas in the disk carries black holes deeper toward the galactic center where they form binary and eventually merge (e.g. Begelman, Blandford & Rees 1980, Escala et al. 2005, Kazantzidis et al. 2005, Dotti et al. 2007). We model both effects as follows:

The time for a satellite to sink to the center of a primary can be approximated using Chandrasekhar dynamical friction (Binney & Tremaine 1987):

$$t_{\text{chandra}} = \frac{1.17 r_{\text{circ}}^2 v_c \epsilon^{\alpha}}{\ln \Lambda \frac{GM_s}{G M_p}}, \quad (1)$$

where $\ln \Lambda$ is the Coulomb logarithm, $\ln \Lambda \approx \ln(1 + M_p/M_s)$. To define the satellite orbit, we adopt values suggested by numerical investigations (Colpi et al. 1999) and used in previous semi-analytical work (Volonteri et al. 2003), the eccentricity $\epsilon^{\alpha} = 0.8$, and the circular velocity v_c is determined at $r_{\text{circ}} = 0.6 r_{\text{vir}}$.

Assuming that each merging galaxy carries a massive black hole at the center, t_{fric} , is the merging time for massive black holes when all other processes (3-body scattering, gas dynamical friction, gravitational radiation, etc.) involved in the formation and later shrinking of the black hole binary are efficient and fast. Due to tidal stripping and possible resonant interactions, simulations have shown that the Chandrasekhar formula underestimates the merger time, especially in the case of minor mergers (e.g. Holley-Bockelmann & Richstone 1999, Weinberg 1989). If this is true, then semi-analytic studies of black hole merger rates using a Chandrasekhar formalism for the merger time will overestimate the true number of black hole mergers.

In an effort to better parametrize dynamical friction, Boylan-Kolchin et al. 2008 used N-body simulations to study dark matter halo merging timescales, and confirmed that the Chandrasekhar formalism does underestimate the merger time, by a factor of ≈ 1.7 for $M_p/M_s \approx 10$ and a factor of ~ 3.3 for $M_p/M_s \approx 100$. They propose a fitting formula that accurately predicts the timescale for a satellite to sink from the virial radius to the host halo center:

$$\frac{\tau_{\text{merge}}}{\tau_{\text{dyn}}} = A \frac{(M_{\text{host}}/M_{\text{sat}})^b}{\ln(1 + M_{\text{host}}/M_{\text{sat}})} \exp \left[c \frac{j}{j_c(E)} \right] \left[\frac{r_c(E)}{r_{\text{vir}}} \right]^d, \quad (2)$$

where $b = 1.3$, $c = 1.9$, $d = 1$, $A = 0.216$, circularity $j / j_c(E) = 0.5$, $r_c(E) / r_{\text{vir}} = 0.65$, as defined in Boylan-Kolchin et al. 2008. The dynamical time, t_{dyn} , is given at virial radius as:

$$\tau_{\text{dyn}} \equiv \frac{r_{\text{vir}}}{V_c(r_{\text{vir}})} = \left(\frac{r_{\text{vir}}^3}{GM_{\text{host}}} \right)^{1/2}, \quad (3)$$

where $V_c(r_{\text{vir}}) = (GM_{\text{vir}}/R)^{1/2}$.

Figure 2 shows the dark matter halo merger timescale for each pair of merging halos for each of these two dynamical friction estimates. We have calculated the dark matter halo merger rate with both Chandrasekhar dynamical friction formula and the Boylan-Kolchin numerical fit. After showing the variance in dark matter halo merger rates from using the two expressions for the dynamical friction timescale (figure 3, discussed in section 3), we thereafter use the Boylan-Kolchin timescale for all other calculations.

It is expected that in gas-rich galaxies, dynamical friction from the gas would bring two black holes close enough to form a binary whose orbit would shrink efficiently, passing quickly from a binary in the 3-body scattering phase to one emitting significant gravitational radiation (Escala et al. 2005, Kazantzidis et al. 2005, Dotti et al. 2007). Numerical simulations indicate that two black holes will sink from ~ 1 kpc to form a binary with a separation of less than a parsec in ~ 10 Myrs. We incorporate this physics by calculating the dynamical friction timescale from the virial radius to the inner kpc, and then assume that the two black holes merge 10 Myr afterward. In practice, the dynamical friction timescale from equations 1 and 2 from the inner kpc to the bound binary stage is often of order 10 Myr; the power of this gas-rich assumption lies in that it entirely circumvents the so-called 'final-parsec' problem thought to exist for low mass ratio mergers of $10^{6.5} M_{\odot} \leq M_{\text{BH}} \leq 10^8 M_{\odot}$ within static, spherical, gas-poor galaxy models (e.g. Milosavljevic & Merritt 2003). We explicitly assume that the black holes in our simulation do not stall at the final parsec before merger, and instead are ushered efficiently into the gravitational radiation stage, where they coalesce; this assumption is verified even in the case of gas-poor galaxy models as long as the model is not spherical or in equilibrium (e.g. Holley-Bockelmann & Sigurdsson 2006, Berczik et al. 2006, R. Spurzem, private communication). Note that this implies that if we assume that each halo initially carries a black hole at its center, and that each host galaxy is gas-rich, figure 2 also estimates the time for a black hole to sink from the virial radius to the center of the host galaxy, become a bound black hole binary, and inspiral due to gravitational radiation.

In our initial work (Micic et al. 2007), mergers of dark matter halos trigger the immediate merger of the black holes they are hosting. In this paper, subsequent mergers of the central black holes are delayed to account for dynamical friction of the halos and the black holes within the galaxy. Black holes will not merge if their merger time is larger than a Hubble time, and in that case, we advance the black hole position within the primary halo at each timestep. Knowing the dynamical friction timescale for each merger, we postpone the black hole mergers by moving them down the merger tree. For the final kpc, we assume that the ambient gas and non-sphericity will cause two black holes to coalesce within 10 Myrs.

2.4 SMBH Growth Prescription

The SMBH in our model grows through a combination of black hole mergers and gas accretion. To better separate the effects of gas accretion on the black hole, we include a dry growth scenario, where the black hole grows through mergers only. To review the approach we have taken in a previous paper, we assumed that major galaxy mergers would funnel gas to the black hole in each of the progenitors and activate an Eddington-limited growth phase for a Salpeter time. Here, the black hole mass would grow as: $M_{\text{BH}}(t) = M_{\text{BH},0}(t_0) \exp(\Delta t/t_{\text{sal}})$, where $\Delta t = t - t_0$, $t_{\text{sal}} \equiv \epsilon M_{\text{BH}} c^2 / [(1 - \epsilon)L]$, ϵ is the radiative efficiency, L is the luminosity, and c is the speed of light; in this picture the black hole mass would roughly double in 40 Myr (Hu et al. 2006). We distinguished two cases depending on the mass ratio of merging dark matter halos. The first is a more conservative criterion that allows black holes to accrete gas if the mass ratio of the host dark matter halo is less than 4:1. The second case sets an upper constraint on the final black hole mass by allowing gas accretion as long as the merging dark matter halos have a mass ratio less than 10:1 – on the cusp of what is considered a minor merger. Since our black holes merged promptly after the halos merged, the accretion timescale and efficiency for major mergers was the same regardless of the mass ratio or redshift.

In this paper, we continue to model the black hole growth as one of extended gas accretion excited by major mergers. At high redshift, this is likely a good assumption, though note that at low redshift when mergers are infrequent, secular evolution, such as bar instabilities, may dominate the gas (and therefore black hole) accretion. Integrated over the whole of a black hole lifetime, though, this major merger-driven accretion is likely to be the dominant source of gas inflow. Since the black hole growth is so strongly dependent on what fuel is driven to the center during galaxy mergers, it is important to characterize this merger-driven gas inflow, including the critical gas physics that may inhibit or strengthen this nuclear supply. We are motivated by a recent suite of numerical simulations that include radiative gas cooling, star formation, and stellar feedback to

study the starburst efficiency for unequal mass ratio galaxy mergers (Cox et al. 2008), which finds that the gas inflow depends strongly on the mass ratio of the galaxy (see also, e.g., Hernquist 1989, Mihos & Hernquist 1995). This study parametrizes the efficiency of nuclear star formation (i.e. gas supply and inflow), α , as a function of galaxy mass ratio:

$$\alpha = \left(\frac{M_s}{M_p} - \alpha_0 \right), \quad (4)$$

where α_0 defines the mass ratio below which there is no enhancement of nuclear star formation (i.e. gas inflow). Here, the gas accretion efficiency has a maximum of 0.56 for 1:1 halo mergers and falls to zero at α_0 . This parametrization is insensitive to the stellar feedback prescription. We use α to define how efficiently the merger funnels the galaxy's gas to the black hole accretion disk. To be consistent with our previous paper, we adopt two definitions for a major merger: one with a mass ratio of $M_p/M_s = 10$, and one with a mass ratio of 4. We adjust α_0 to deactivate gas accretion below the major merger threshold. In Cox et al. 2008, the fitted α_0 parameter suggests a nuclear starburst cut off for mass ratios larger than 9. Note that the Cox et al. 2008 study does not include the important effect of black hole feedback, which will shut off gas inflow after a merger.

Now that we have a more realistic description of the merger time for each black hole within a halo, we allow them to grow for a physically-motivated accretion timescale. The accretion of gas onto both incoming and central black hole starts when the two black holes are still widely separated, at the moment of the first pericenter passage, and continues until the black holes merge (c.f. Di Matteo et al. 2005, Colpi et al. 2007). This sets the accretion timescale, t_{acc} , as follows: $t_{\text{acc}} = t_{\text{df}}(r=R_{\text{vir}}) - t_{\text{dyn}}(r=R_{\text{vir}})$, where $t_{\text{df}}(r=R_{\text{vir}})$ is the merger timescale including dynamical friction; and $t_{\text{dyn}}(r=R_{\text{vir}})$ is dynamical time at virial radius R_{vir} , which marks the first pericenter pass of the black hole. By stopping the accretion as the black holes merge, we roughly model the effect of black hole feedback in stopping further accretion.

Putting these pieces together, the mass accreted by a black hole during $t_{\text{acc}}(r=R_{\text{vir}})$ is:

$$M_{\text{acc}} = M_{\text{BH},0} \left(e^{\frac{\alpha t_{\text{acc}}}{t_{\text{sal}}}} - 1 \right), \quad (5)$$

where $M_{\text{BH},0}$ is initial black hole mass, and α is starburst efficiency (Cox et al. 2008), and t_{sal} is defined above. After t_{df} , the incoming black hole merges with the SMBH at the center and a new SMBH is formed after having accreted gas for t_{acc} . The accretion time and efficiency both implicitly encode the large-scale dynamics of the merger and the bulk gas accretion into the nuclear region, while t_{sal} describes the accretion disk physics. As before, we set t_{sal} to describe sustained Eddington-limited accretion with a efficiency of 0.1 (Shakura & Syunyaev 1973).

3 RESULTS

Black hole mergers postponed for longer than the Hubble time will not occur, which reduces the merger rate over all redshifts. In the absence of dynamical friction, there are 1447 black hole mergers in our volume between redshifts 20 and 0; this number reduces to 1248 with Chandrasekhar dynamical friction, and 1063 with a Boylan-Kolchin estimate for the dynamical friction decay time.

The number of dark matter halo mergers per unit redshift per year is presented in figure 3 (thick line). This halo merger rate directly corresponds to the black hole merger rate when the black holes merge immediately after their host halos. When Chandrasekhar dynamical friction is introduced to the black hole merger tree (figure 3, dashed line) the black hole merger rates decrease over all redshifts except at $z \leq 2.7$, as the mergers that have been delayed from higher redshift begin to occur. The black hole merger rate is maximum at $z=11$ without dynamical friction, and at this redshift the rate decreases by a factor of 1.5 for Chandrasekhar dynamical friction. This reduction in the black hole merger rate is even more pronounced when we use the Boylan-Kolchin equation for the merger timescale (figure 3, dotted line), dropping the merger rate by a factor of two.

Those mergers that are postponed but have a merging timescale less than a Hubble time will be pushed down the merger tree toward lower redshifts. This is made explicit in figure 4, which plots the average change in redshift for a merger as a function of redshift if one includes dynamical friction. Black hole mergers at redshift 10 are, on average, pushed to redshift 6, for example. This results in an increase in the black hole merger rate at low redshifts. We can see this clearly in figure 3; although the maximum merger rate at redshift $z=11$ has dropped, the number of mergers is larger than the Chandrasekhar merger rate at $z \leq 6$ (and therefore also larger than without dynamical friction at $z \leq 2.7$). Again, this is because dynamical friction postpones mergers longer with the Boylan-Kolchin formula. This suggests higher LISA merger rates at low redshifts than any estimate that used the Chandrasekhar formula. In addition, since each merger occurs at a lower redshift, it will certainly be a louder gravitational wave source, and any associated electromagnetic signature will be brighter, as well. We will return to the LISA detectability in a future paper.

Interestingly, including dynamical friction from gas at distances smaller than 1 kpc does not make difference in our merger rates. Those black holes that reach 1 kpc from the galactic center will reach a parsec even without the gas – the gas timescale is simply invoked to ensure that the black holes pass through the 3-body scattering stage efficiently. For the rest of this paper, we adopt the Boylan-Kolchin dynamical friction fit as a realistic treatment of the black hole merger timescale.

In order to address the effect of inefficient black hole seed formation on the black hole merger rates, we randomly seed only 10% of those halos that could host a Pop III star with a $200 M_{\odot}$ black hole. We ran 100 realizations of this process, applying Boylan-Kolchin merger timescales as described above. These rates are presented at the bottom of figure 3 with maximum of range $2 - 3 \text{ yr}^{-1}$. This is a pessimistic scenario since it suggests that only 10% of dark matter halos are capable of hosting a seed black hole. Future work on this subject will give more realistic predictions for Pop III seeding efficiency, but we point out that even with our lowest estimate for the number of black hole seeds, the predicted LISA merger rate of $2 - 3 \text{ yr}^{-1}$ makes this population a reliable gravitational wave source.

By design of our small volume simulation, we have only one SMBH in our volume sitting a halo with $3 \times 10^{12} M_{\odot}$, roughly the mass of the Milky Way halo. Figure 5 shows the SMBH mass at the center of the primary halo as a function of redshift. SMBH growth without dynamical friction is presented with thin lines for the three scenarios (dry growth, 4:1 growth, and 10:1 growth) described previously. The thick lines present corresponding growth models with dynamical friction. The first merger of the primary dark matter halo with a satellite occurs at redshift $z=14.2$; without dynamical friction, that is also the redshift of the first black hole merger. This merger is postponed until $z=11.7$ when dynamical friction is added. In our model, major mergers are followed by the episodes of gas accretion which can be identified in figure 5 as rapid increases in the SMBH mass. A great example of how SMBH mergers are postponed by dynamical friction can be seen in the change in SMBH mass for the redshift range $4.7 \leq z \leq 6.1$. Although the last major merger of the primary halo is at $z=6.1$ (figure 5, thin dash-dot line), the SMBH at the center of the primary halo undergoes at least three rapid increases in mass in the 10:1 growth model (figure 5, thick dash-dot line) for the redshift range $4.7 \leq z \leq 6.1$. These are from satellite mergers originating at higher redshift. Redshift 4.7 marks the end of the gas accretion era for the SMBH, well after it experiences its last major merger. The SMBH is close to its final mass at this time, as the only channel left in our model for increasing its mass is via black hole mergers. We note that the 10 next most massive black holes all reach their final mass at varying redshifts between 10 and 1, though in our volume, these black holes are $10^3 - 10^5 M_{\odot}$.

The range for the SMBH mass set by the 4:1 and 10:1 dynamical friction growth models is $1.7 \times 10^6 M_{\odot} \leq M_{\text{SMBH}} \leq 1.3 \times 10^7 M_{\odot}$. If we neglect dynamical friction, the black hole masses are unphysically large. Dynamical friction removes 27% of the total number of initially merging black holes because these will take longer than a Hubble time to coalesce. All other black holes merge later, and these effects both prevent the seed from accumulating a large mass early on to use as a 'base' for Salpeter accretion phases. The effect of delaying and removing the mergers outweighs the longer accretion timescales seen when dynamical friction is included.

Figure 6 shows the universal merger rates for those dark matter halos that merge in less than a Hubble time within the mass range $10^7 M_{\odot} \leq M_{\text{DMH}} \leq 10^{12} M_{\odot}$, for various mass ratios and combined masses of merging dark matter halos. Black holes seeded in halos in the middle and bottom panels grow through mergers only and never accrete, while gas accretion impacts black hole growth in 4:1 and 10:1 halo mergers (figure 6, upper panel). In our volume, all the mergers that occur at redshifts $z \leq 2$ will not finish in less than a Hubble time, as these mergers are all high mass ratio. We remind the reader, though, that these halo merger rates are extrapolated from our 10 Mpc simulation box; a better global rate for these low mass halos will be achieved with more of these volumes.

Since the merger timescale is larger for higher mass ratio halos, the black hole gas accretion time scale is longer, as well. Figure 7 shows the gas accretion time scale for black holes hosted by dark matter halos that merge with mass ratio $M_{\text{DMH1}}/M_{\text{DMH2}}$ and combined mass $p=\log(M_{\text{DMH1}}+M_{\text{DMH2}})$. Notice that gas accretion is activated only for a small range of halo mass ratios $M_{\text{DMH1}}/M_{\text{DMH2}} \leq 10$. For these mergers, the black holes do not accrete for longer than ~ 1000 Myr, and the accretion efficiency is strongly damped as the halo mass ratio tends toward 10:1.

The number of accreting black holes as a function of redshift is presented in figure 8. The thick line represents the 10:1 growth case, and this also corresponds to halos with mass ratio $M_{\text{DMH1}}/M_{\text{DMH2}} \leq 10$ in figure 7. In the same manner, the thin line (4:1 growth) corresponds to halos with mass ratio $M_{\text{DMH1}}/M_{\text{DMH2}} \leq 4$ in figure 7. In either accretion scenario, the number of accreting black holes reduces by ~ 200 at redshift 4.7, from a few hundred accreting black holes to a few tens. This corresponds to the redshift at which the SMBH at the center of the primary halo stops accreting gas from the previous major merger. Those black holes that are still accreting gas at $z \leq 4.7$ are mostly rogue black holes at the outskirts of the primary halo. We will discuss these more in the next subsection.

The last episode of gas accretion by the SMBH is also an epoch during which the SMBH accumulates largest amount of mass. Figure 9 shows the rate of mass growth of the SMBH for 10:1 growth with (thick line) and without (thin line) dynamical friction. At the redshift of the last gas accretion, $z \sim 4.7$, the mass growth rate is $\sim 1 M_{\odot}/\text{year}$ for 10:1 growth with dynamical friction. Thereafter, the gas accretion is extremely damped; although this SMBH is far too low mass to be considered a high luminosity AGN analogue, it may be appropriate to link this SMBH with a low luminosity AGN (Ho 2008).

We divide the universal black hole merger rates as a function of redshift in figure 10 into different binary mass ratios and total binary mass ranges, where $p = \log(m_1 + m_2)$ is a measure of the total binary black hole mass. Horizontally, we separate the merger rate by mass ratio: in panels a, b, and c, we focus on $1 \lesssim m_1/m_2 < 10$; $10 \lesssim m_1/m_2 < 100$ in d, e, f; and $100 \lesssim m_1/m_2 < 10000$ in g, h, i. Each column represents a different black hole growth scenario: we cover dry growth in a, d, g; 4:1 growth in b, e, h; and 10:1 growth in c, f, i. The black hole mass ratio of $100 \lesssim m_1/m_2 < 10000$ corresponds to

SMBH/IMBH mergers, and the merger rate is $3 - 7 \text{ yr}^{-1}$ for both the 4:1 case (h) and 10:1 case (i), between redshifts 1 and 5. Assuming that before the merger occurs, the incoming IMBH behaves as ULX source, the expected frequency of ULX sources would also be $\sim 3 - 7 \text{ yr}^{-1}$. These black hole mergers have the appropriate total mass to be important LISA sources. We will return to the integrated LISA signal, event rates, and source characterization in a future paper.

3.1 Rogue Massive Black Holes

Over the span of the simulation, the primary accretes 483 satellite halos total, and 382 of them have orbital decay times that are longer than a Hubble time (see figure 11 for the merger rate and mass ratios of these halos). By redshift zero, then, these halos are still orbiting at significant distances from the primary center – and although the halos themselves have been stripped by the primary potential, they are still embedded with massive black holes. Figure 12 displays the number of these ‘rogue’ black holes as a function of the distance from the primary center at redshift zero. For a primary scaled to the Milky Way, this implies that roughly 1-10 of these massive black holes in orbit at the solar radius.

Given the merger-driven accretion scenario described in the previous section, we can determine the mass of these black holes at redshift zero. Figure 13 shows the mass of each rogue as a function of distance from the primary center; each black hole is color-coded to keep track of when the satellite halo entered the virial radius of the primary. Note that the most massive of these black holes are embedded in satellites that have themselves undergone mergers before entering the primary halo at redshift $2 < z < 4$. This ‘preprocessing’ via prior mergers allows the black holes to enter the primary halo at later times with higher masses; these most massive rogues remain at roughly half the virial radius by redshift zero.

There is sufficient evidence that the halos of galaxies, from massive ellipticals to isolated spirals, can host diffuse hot halo gas (Matthews & Brighenti 2003, O’Sullivan 2001, Pedersen et al. 2006). As these black holes orbit within the primary halo, they can accrete from this ambient hot halo gas via Bondi-Hoyle accretion. Here, the mass accretion rate can then be described by:

$$\dot{M}_{\text{BH}} = \frac{4\pi G^2 M_{\text{BH}}^2 \rho_{\text{ISM}}}{(c_s^2 + v^2)^{3/2}}, \quad (6)$$

where ρ_{ISM} is the density of the halo gas, c_s is the gas sound speed, and v is the velocity of the black hole. For these rogue black holes, we add this more quiescent form of accretion from the time the black hole has entered the virial radius of the halo in order to determine whether any of these rogue black holes may be visible today. To model the hot halo gas, we assume it has an isothermal density profile consistent with X-ray observations of halo gas in ellipticals (Matthews & Brighenti 2003), and that the ideal gas is in hydrostatic equilibrium with the gravitational potential of the halo. We assume a gas core radius of $0.3R_s$, where R_s is the scale radius of the NFW halo, and that the gas temperature is the virial temperature at the virial radius. This yields a central gas temperature of $\sim 2 \times 10^6 K$ for a dark matter halo of mass $2 \times 10^{12} M_\odot$, which is also consistent with observations (Pedersen et al. 2006). At redshift zero, we assume the black holes are on bound elliptical orbits of eccentricity 0.8 to match simulation predictions for satellite mergers (e.g. Ghigna et al. 1998, Sales et al. 2007).

By redshift zero, a black hole will have grown to a new mass M_{rogue} , and will have a new accretion rate from equation 6. The radiated luminosity from this process can be determined from $L_{\text{rogue}} = \eta \dot{M}_{\text{BH}} c^2$, where η describes how efficiently mass is converted to energy; the standard assumption for an accretion disk around a spinning black hole sets $\eta \sim 0.1$ (Shakura & Syunyaev 1973). We find that our most massive rogue black holes can radiate at $\sim 10^4 L_\odot$ (figure 14), making them somewhat fainter than the brightest ULXs; the fact that the hot halo gas is so tenuous at these radii is what accounts for the relatively low luminosity. However, if these rogue black holes are common, they will be observable in the outskirts of the Milky Way halo with Chandra, and the most luminous can have sufficient signal-to-noise for spectral characterization. Note, though, that a significant fraction of these may have advection-dominated accretion flows, rather than proper accretion disks, and hence η may be much less than 0.1; this would naturally make the black hole less luminous, but with a harder spectral signature. Even if they are not observable electromagnetically, they may be detected by mesolensing (di Stefano 2007).

3.2 Low Mass Black Hole Demography

For dark matter halo masses above roughly $5 \times 10^{11} M_\odot$, the dark matter halo mass correlates well with the mass of the supermassive black hole (Ferrarese 2002):

$$\frac{M_{\text{BH}}}{10^8 M_\odot} \sim 0.10 \left(\frac{M_{\text{DMH}}}{10^{12} M_\odot} \right)^{1.65}, \quad (7)$$

where M_{DMH} is the dark matter halo mass. Below this mass, there is tentative evidence that halos are less effective at forming massive black holes, and may even be unable to form them (Ferrarese 2002). To be fair, though, if this relation does hold down to a $10^{11} M_\odot$ halo, the expected $2 \times 10^4 M_\odot$ black hole would be difficult to detect, observationally.

In our volume, there are few halos with masses $\geq 10^{11} M_{\odot}$ by redshift zero, so our sample is limited. However, we can still find the final black hole and halo mass for every black hole that has undergone some accretion by redshift zero. This is plotted in figure 15. Notice that our single SMBH in the volume is consistent with the $M_{\text{BH}} - M_{\text{DM}}$ relation for a 10:1 growth scenario, and many of our lower mass black holes do as well. There are a few tidally-stripped satellite halos on the low mass end that host overweight black holes. In addition, those dark matter halos with sparse merger histories host underweight black holes. This may point to a dependence of the black hole mass on environment. We will be able to explore this more carefully with the set of simulations currently underway.

3.3 Comparison to Published Black Hole Merger Rates

Previous work on black hole merger rates use semi-analytical models based on Extended Press-Schechter theory (EPS), and the dynamical friction in these models uses the Chandrasekhar formalism. We compare our results with those obtained from EPS theory. Figure 16 shows the merger rates for four Press-Schechter models described in Sesana et al. 2007. In the VHM model, massive DMHs ($M_{\text{DMH}}=10^{11} - 10^{15} M_{\odot}$) are seeded with $m_{\text{BH}}\sim 200 M_{\odot}$ black holes at $z=20$; in the KBD model, low mass halos ($M_{\text{DMH}}=10^6 - 10^7 M_{\odot}$) are seeded with $m_{\text{BH}}\sim 5\times 10^4 M_{\odot}$ at $15\lesssim z\lesssim 20$; and the BVR models explore different redshift ranges for seeding black holes within halos: $m_{\text{BH}}=10^4 - 10^5 M_{\odot}$ at $15\lesssim z\lesssim 20$ in the BVRhf model and $18\lesssim z\lesssim 20$ in the BVRlf model. Our black hole merger rate is overplotted in thick black. The best match to our model is the KBD model, though their seed black holes are more massive. This match is not surprising since the range of seeding redshifts and the halo mass range are similar to ours. Our merger rate at high redshift is larger because we seed black holes in a wider mass range of dark matter halos. At $z \leq 11$, however, KBD merger rates are larger since they use Chandrasekhar dynamical friction, which underestimates the merger timescale. This simple rate comparison of merger rates, however, neglects the larger differences in black hole masses and the mass ratio of each merger.

4 DISCUSSION

Using a small volume cosmological n-body simulation to construct the merger history of low mass dark matter halos, we have studied the growth and merger rate of black holes from seeds at redshift 20 to low mass SMBHs at redshift zero, analytically incorporating the important sub-resolution physics to model the black hole dynamics and gas accretion. We found that the method used to estimate the dynamical friction timescale makes a large difference in the total rate and redshift distribution of black hole mergers; for example, the merger rate is smaller at higher redshift $z \geq 6$ with an n-body based dynamical friction estimate (Boylan-Kolchin 2008) than with the Chandrasekhar dynamical friction approximation, because this approximation underestimates the true merger time. If most of the black hole growth is tied to gas accretion that is activated by major mergers, then using the Chandrasekhar dynamical friction approximation will overestimate the mass of the black hole. Moreover, these larger, more realistic merger timescales will postpone black hole mergers to lower redshifts, which increases the black hole merger rate at $z \leq 6$.

We find that the maximum black hole merger rate is $R \sim 25\text{yr}^{-1}$ at $z \sim 10\text{yr}^{-1}$. However, when a Pop III seed formation efficiency of 0.1 is adopted, the maximum merger rate falls to $R \sim 3\text{yr}^{-1}$. This scenario is based on the most pessimistic picture of the evolution of the first stars; future work will constrain the occupation fraction of seed black holes. However, even with such a low Pop III formation efficiency, and a larger merger timescale than has previously been used, the merger rate is large enough for SMBH mergers to remain an important LISA source.

We also introduce an expression for the growth of a black hole that includes direct mergers of the black hole and Eddington-limited accretion driven by major mergers. We use the merger time starting from the first pericenter passage of the incoming black hole to set the gas accretion timescale, and we weighted the efficiency of accretion by the available gas in the galaxy nucleus, which has been carefully studied for unequal mass galaxy mergers (Cox et al. 2008). With this black hole growth scenario, we find that if we define a major merger as one with a 4 : 1 halo mass ratio, the final SMBH mass at the center of a Milky Way type halo is $M_{\text{BH}} = 1.7\times 10^6 M_{\odot}$. If, instead, we adopt a more lenient definition of a major merger (10:1), $M_{\text{BH}} = 1.3\times 10^7 M_{\odot}$. This first value is similar to the mass of the SMBH observed at the center of our Galaxy, while the second is consistent with the mass at the center of M31. Hence, we have shown in this study that not only is it possible to grow these low mass SMBHs from very light Pop III remnants, but that most of the SMBH mass can be accounted for with a combination of major merger-driven gas accretion and direct black hole mergers.

We emphasize that with a growth prescription that is so strongly tied to major galaxy mergers, it is possible to have low mass black holes in place at high redshift and not accreting strongly thereafter. In fact, the most massive black hole in our small volume grew most rapidly for a short span around redshift 4.5; thereafter, it was quiescent. This may seem in direct contradiction to previous observational studies that have argued for the ‘‘anti-hierarchical’’ growth of black holes, meaning that the most massive SMBHs accrete most at high redshift, while the lower mass SMBHs are still accreting (and grow the most) at $z < 1$ (Merloni 2004, Marconi et al. 2004). This apparent contradiction may not be so clear, however. First, the

black holes in our volume were lower mass than what is typically considered in the local census of relic AGN. Second, these observational studies are based on linking the observed local black hole mass function to high redshift AGN assuming that these black holes grow only by gas accretion (and not merging) with a single accretion efficiency. Our black holes would not be able to grow to $10^6 M_{\odot}$ without a rich merger history. Third, our simulations do not explicitly include any of the more 'quiescent' black hole growth modes, such as bar-driven gas inflow, stellar tidal disruption, compact object capture, and sub-Eddington Bondi-Hoyle-Littleton accretion from the surrounding gaseous medium. These may very well act to increase the growth rate of some of the black holes in our simulation at lower redshift¹. However, if this form of growth were to dominate at $z < 1$ for the SMBH in our volume, the SMBH would be too massive. Finally, we appeal to cosmic variance; our volume was selected to be a sparse group environment, and as such, SMBHs were rare. If galaxy merger-driven inflow, direct black hole mergers, and these more quiescent forms of black hole accretion all play roles in the assembly of low mass SMBHs, each growth channel may have a different strength as a function of environment. We are running several high-resolution, small volume simulations to tackle this issue.

In this paper, we have neglected gravitational wave recoil, a potentially important mechanism that may inhibit black hole growth. Binary black holes strongly radiate linear momentum in the form of gravitational waves during the plunge phase of the inspiral – resulting in a “kick” to the new black hole. This, in itself, has long been predicted as a consequence of an asymmetry in the binary orbit or spin configuration. Previous kick velocity estimates, though, were either highly uncertain or suggested that the resulting gravitational wave recoil velocity was relatively small, astrophysically speaking. Now, recent results indicate the recoil can drive a gravitational wave kick velocity as fast as $\sim 4000 \text{ km s}^{-1}$ (Herrmann et al. 2007; Gonzalez et al. 2007a, 2007b; Koppitz et al. 2007; Campanelli et al. 2007, Schnittman & Buonanno 2007). In reality, much smaller values than this maximum may be expected in gas-rich galaxies due to the alignment of the orbital angular momentum and spins of both black holes (Bogdanovic et al. 2007). However, even typical kick velocities ($\sim 200 \text{ km s}^{-1}$) are interestingly large when compared to the escape velocity of typical astronomical systems - low mass galaxies, as an example, have an escape velocity of $\sim 200 \text{ km s}^{-1}$ (e.g. Holley-Bockelmann et al. 2007). The effect of large kicks combined with low escape velocity from the centers of small dark matter halos at high redshift plays a major role in suppressing the growth of black hole seeds into SMBH. Even the most massive dark matter halo at $z \geq 11$ can not retain a black hole that receives $\geq 150 \text{ km s}^{-1}$ kick (Merritt et al. 2004, Micic et al. 2006). In our next paper we will incorporate the effect of recoil velocity on the expected merger rates and the growth of the SMBH.

ACKNOWLEDGMENTS

REFERENCES

- Aguilar, L. A., & White, S. D. M. 1986, *ApJ*, 307, 97
 Alexander, D.M., Smail, I., Bauer, F.E., & Chapman, S.C., Blain, A.W., Brandt, W.N., Ivison, R.J., 2005, *Natur*, 434, 738A
 Aller M.C., Richstone D., 2002, *AJ*, 124, 3035
 Abel, T., Bryan, G., & Norman, M., 2000, *ApJ*, 540, 39
 Abel, T., Bryan, G., & Norman, M., 2002, *Sci*, 295, 93A
 Adams, F.C., Graff, D.S., Richstone, D.O., 2001, *ApJ*, 551L, 31A
 Baes, M., Buyle, P., Hau, G.K.T., Dejonghe, H., 2003, *MNRAS*, 341L, 44B
 Barth, A.J., Ho, L.C., Rutledge, R.E., Sargent, W.L.W., & 2004, *ApJ*, 607, 90B
 Begelman, M.C., & Blandford, R.D., Rees, M.J., 1980, *Natur*, 287, 307
 Begelman, M.C., Rees, M.J., 1978, *MNRAS*, 185, 847B
 Bender, R., Kormendy, J., Bower, G., 2005, *ApJ*, 631, 280
 Bennett, C.L., et al., 2003, *ApJ*, 148, 1
 Berczik, P., Merritt, D., Spurzem, R., Bischof, H.P., & 2006, *ApJ*, 642L, 21B
 Binney, J., Tremaine, S., 1987, *Galactic Dynamics* & (Princeton: Princeton Univ. Press)
 Bogdanovic, T., Reynolds, C.S., Miller, M.C., & 2007, *ApJ*, 661L, 147B
 Boylan-Kolchin, M., Ma, C.P., Quataert, E., & *MNRAS*, 383, 93B
 Bromm, V., Coppi, P.S., & Larson, R.B., 1999, *ApJ*, 527, L5
 Bromm, V., Loeb, A., 2003, *ApJ*, 596, 34B
 Bromm, V., Loeb, A., 2004, *NewA*, 9, 353B
 Bullock, J.S., Kollat, T.S., Sigad, Y., Somerville, R.S., & Kravtsov, A.V., Klypin, A.A., Primack, J.R., Dekel, A., 2001, *MNRAS*, 321, 559B
 Burkert, A., Silk, J., 2001, *ApJ*, 554L, 151B
 Campanelli, M., Lousto, C.O., Zlochower, Y., Merritt, D., 2007, *gr.qc*, 2133C
 Cattaneo, A., Haehnelt, M.G., Rees, M.J., 1999, *MNRAS*, 308, 77C
 Colpi, M., Mayer, L., Governato, F., 1999, *ApJ*, 525, 720C
 Colpi, M., Dotti, M., Mayer, L., & Kazantzidis, S. 2007, *ArXiv e-prints*, 710, arXiv:0710.5207

¹ They also may have little effect: a recent study by Ho, Filippenko & Sargent (1997) found that there barred galaxies do not increase the strength or frequency of the AGN

- Cowie, L.L., Barger, A.J., Bautz, M.W., & Brandt, W.N., Garmire, G.P., 2003, *ApJ*, 584, L5
- David, L.P., Durisen, R.H., Cohn, H.N., 1987, *ApJ*, 313, 556D
- Davis, M., Efstathiou, G., Frenk, C., White, S.D.M., & 1985, *ApJ*, 292, 371
- Dehnen, W., McLaughlin, D.E. & Sachania, J., 2006, *MNRAS*, 369, 1688
- Di Matteo, T., Croft, R.A.C., Springel, V., & Hernquist, L., 2003, *ApJ*, 593, 56D
- Di Matteo, T., Springel, V., Hernquist, L., 2005, *Natur*, 433, 604D
- Di Stefano, R., 2007, *astro-ph/0712.3558*
- Dotti, M., Colpi, M., Haardt, F., Lucio, M., 2007, *MNRAS*, 379, 956D
- Ebisuzaki, T., Makino, J., Okumura, S.K., 1991, *Natur*, 354, 212E
- Erickcek, A.L., Kamionkowski, M., & Benson, A.J., 2006, *MNRAS*, tmp, 940E
- Escala, A., Larson, R.B., Coppi, P.S., & Mardones, D., 2005, *ApJ*, 630, 152E
- Fabbiano, G., 1989, *ARA&A*, 27, 87
- Fabbiano, G., White, N.E., 2006, & in *Compact Stellar X-Ray Sources*, ed. W. H. G. Lewin & M. van der Klis & (Cambridge: Cambridge Univ. Press), 475
- Fan, X., 2005, *gbha.conf*, 75F
- Ferrarese, L., Merritt, D., 2000, *ApJ*, 539L, 9F
- Ferrarese, L., 2002, *ApJ*, 578, 90F
- Filippenko, A.V., Ho, L.C., 2003, *ApJ*, 588L, 13F
- Gao, L., White, S.D.M., Jenkins, A., Frenk, C.S., Springel, V., & 2005, *MNRAS*, 363, 379
- Gebhardt, K., et al. 2000, 539L, 13G
- Gebhardt, K., Rich, R.M., Ho, L.C., 2005, *ApJ*, 634, 1093G
- Gehz, A.M., Duchene, G., Matthews, K., 2003, *ApJ*, 586, 127
- Gehz, A.M., Salim, S., Hornstein, S.D., 2005, *ApJ*, 620, 744
- Ghigna, S., Moore, B., & Governato, F., Lake, G., Quinn, T., Stadel, J., 1998, *MNRAS*, 300, 146
- Gonzalez, J.A., Hannam, M., Spherhake, U., Bruggmann, B., Husa, S., 2007, *PhRvL*, 98w1101G
- Gonzalez, J.A., Spherhake, U., Bruggmann, B., Hannam, M., Husa, S., 2007, *PhRvL*, 98i1101G
- Granato, G.L., Silva, L., Monaco, P., Panuzzo, P., & Salucci, P., De Zotti, G., Danese, L., 2001, *MNRAS*, 324, 757G
- Green, J.E., Ho, L.C., 2004, *ApJ*, 610, 722G
- Greenstein, J.L., Matthews, T.A., 1963, *AJ*, 68S, 279G
- Haehnelt, M.G., 1994, *MNRAS*, 269, 199
- Haehnelt, M.G., Kauffmann, G., 2000, *MNRAS*, 318L, 35H
- Haehnelt, M.G., Natarajan, P., Rees, M.J., 1998, *MNRAS*, 300, 817H
- Heckman, T.M., Kauffmann, G., Brinchmann, J., & Charlot, S., Tremonti, C., White, S.D.M., 2004, *ApJ*, 613, 109
- Heger, A., Woosley, S.E., 2002, *ApJ*, 567, 532H
- Heger et al., 2003, *ApJ*, 591, 288H
- Heggie, D.C., Hut, P., Mineshige, S., Makino, J., & Baumgardt, H., 2007, *PASJ*, 59L, 11H
- Hernquist, L., 1989, *Natur*, 340, 687
- Hernquist, L., & Mihos, J.C., 1995, *ApJ*, 448, 41
- Herrmann, F., Hinder, I., Shoemaker, D., Laguna, P., & Matzner, R.A., 2007, *ApJ*, 661, 430H
- Ho, L., 2008, *astro-ph/0803.2268*
- Ho, L.C., Filippenko, & A.V., Sargent, W.L.W., 1997, *ApJ*, 487, 591
- Holley-Bockelmann, K., Gultekin, K., Shoemaker, D., & Yunes, N. 2007, *ArXiv e-prints*, 707, *arXiv:0707.1334*
- Holley-Bockelmann, K., & Sigurdsson, S., 2006, *astro-ph*, 1520H
- Holley-Bockelmann, K., & Richstone, D.O., 1999, *ApJ*, 517, 92H
- Hopkins, P.F., Hernquist, L., Cox, T.J., Di Matteo, T., & Martini, P., Robertson, B., Springel, V., 2005, *ApJ*, 630, 705H
- Hu, J., Shen, Y., Lou, Y., Zhang, S., 2006, *ApJ*, 365, 345
- Islam, R. R., Taylor, J. E., Silk, J., & 2003, *MNRAS*, 340, 647I
- Islam, R. R., Taylor, J. E., Silk, J., & 2004, *MNRAS*, 354, 427I
- Kauffmann, G., Haehnelt, M., 2000, *MNRAS*, 311, 576K
- Kazantzidis, S., Mayer, L., Colpi, M., & Madau, P., Debattista, V.P., Wadsley, J., Stadel, J., Quinn, T., Moore, B., & 2005, *ApJ*, 623L, 67K
- King, A.R., Davies, M.B., Ward, M.J., Fabbiano, G. & Elvis, M., 2001, *ApJL*, 552, 109
- Koppitz, M., Pollney, D., Reisswig, C., Rezzolla, L., & Thornburg, J., Diener, P., Schnetter, E., 2007, *gr.qc*, 1163K
- Kormendy, J., Richstone, D., 1995, *ARA&A*, 33, 581K
- Koushiappas, S.M., Bullock, J.S., Dekel, A., 2004, *MNRAS*, 354, 292K
- Lacey, C., Cole, S., 1993, *MNRAS*, 262, 627
- Lehmer, B.D., Brandt, W.N., Hornschemeier, A.E., & Alexander, D.M., Bauer, F.E., Koekemoer, A.M., Schneider, D.P., Steffen, A.T., & 2006, *AJ*, 131, 2394L
- Loeb, A., Rasio, F.A., 1994, *ApJ*, 432, 52L
- Machacek, M.E., Bryan, G.L., & Abel, T. 2001, *ApJ*, 548, 509
- Mack, K.J., Ostriker, J.P., Ricotti, M., *astro-ph/0608642*
- Madau, P., Rees, M.J., 2001, *ApJ*, 551L, 27M
- Makino, J., 1997, *ApJ*, 478, 58M
- Marconi, A., Risaliti, & G., Gilli, R., Hunt, L.K., Maiolino, R., Salvati, M., 2004, *MNRAS*, 351, 169
- Mayer, L., Kazantzidis, S., Madau, P., Colpi, M., & Quinn, T., Wadsley, J., 2007, *Sci*, 316, 1874M
- Menou, K., Haiman, Z., Narayanan, V.K., & 2001, *ApJ*, 558, 535
- Merloni, A., 2004, *MNRAS*, 353, 1035
- Merritt, D., Ferrarese, L., 2001, *ApJ*, 547, 140M

- Merritt, D., Milosavljevic, M., Favata, M., Hughes, S.A., Holz, D.E., 2004, ApJ, 607L, 9M
Mihos, J.C., Hernquist, L., 1994, ApJ, 425L, 13M
Mii, H., Totani, T., 2005, ApJ, 628, 873
Miller, M.C., Colbert, E.J.M., 2004, IJMPD, 13, 1M
Milosavljevic, M., Merritt, D., 2001, ApJ, 563, 34M
Milosavljevic, M., Merritt, D., 2003, ApJ, 596, 860M
Micic, M., Abel, T., Sigurdsson, S., 2006, MNRAS, 372, 1540M
Micic, M., Holley-Bockelmann, K., Sigurdsson, S., Abel, T., 2007, MNRAS, 380, 1533M
Monaco, P., Salucci, P., Danese, L., 2000, MNRAS, 311, 279M
Nagashima, M., et al. 2005, ApJ, 634, 26N
Nakamura, F., Umemura, M., 2001, ApJ, 548, 19N
Navarro, J.F., Frenk, C.S., White, S.D.M., & 1995, MNRAS, 275, 56N
Omukai, K., Yoshii, Y., 2003, ApJ, 599, 746O
Omukai, K., Palla, F., 2003, ApJ, 589, 677O
Omukai, K., Nishi, R., 1998, ApJ, 508, 141O
Portegies Zwart, S.F., Baumgardt, H., Hut, P., & Makino, J., McMillan, S.L.W., 2004, Natur, 428, 724P
Press, W.H., Schechter P., 1974, ApJ, 187, 425
Ptak, A., Colbert, E., 2004, ApJ, 606, 291
Quinlan, G.D., 1996, NewA, 1, 35Q
Reed, D.S., Bower, R., Frenk, C.S., Jenkins, A, Theuns, T., & 2007, MNRAS, 374, 2R
Rees, M.J., 1984, ARA&A, 22, 471R
Rhook, K.J., Wyithe, J.S.B., 2005, MNRAS, 361, 1145
Richstone, D. O. 1976, ApJ, 204, 642
Ripamonti, E., Haardt, F., Ferrara, A., Colpi, M, & 2002, MNRAS, 334, 401R
Robertson, B., Hernquist, L., Cox, T.J., Di Matteo, T., & Hopkins, P.F., Martini, P., Springel, V., 2006, ApJ, 641, 90R
Sales, L.V., Navarro, & J.F., Abadi, M.G., Steinmetz, M., 2007, MNRAS, 379, 1464
Shankar, F., Lapi, A., Salucci, P., De Zotti, G., Danese, L., & 2006, ApJ, 643, 14S
Schneider, R., Ferrara, A., & Natarajan, P., Omukai, K., 2002, ApJ, 571, 30S
Schnittman, J.D., Buonanno, A., 2007, ApJ, 662L, 63S
Seljak, U., 2002, MNRAS, 334, 797S
Sesana, A., Haardt, F., Madau P., & Volonteri, M., 2004, ApJ, 611, 623
Sesana, A., Volonteri, M., Haardt, F., & 2007, astro-ph/0701556
Shakura, N.I., Syunyaev, R.A., 1973, A&A, 24, 337S
Sigurdsson, S., 2003, CQGra, 20S, 45S
Soltan A., 1982, MNRAS, 200, 115S
Silk, J., Rees, M.J., 1998, A&A, 331L, 1S
Spergel, D.N., et al., 2007, ApJ, 170, 377
Springel, V., Yoshida, N., & White, S. D. M., 2001, NewA, 6, 79
Springel, V., 2000, MPA
Taffoni, G., Mayer, L., Colpi, M., Governato, F., 2003, MNRAS, 341, 434T
Tremaine, S., et al. 2002, ApJ, 574, 740T
van der Marel, R.P., 2004, cbhg.symp, 37V
Volonteri, M., Haardt, F., & Madau, P., 2003, ApJ, 582, 559
Wang, J.M., Chen, Y.M., Zhang, F., 2006, ApJ, 647L, 17W
Weinberg, M.D., 1989, MNRAS, 239, 549
Wise, J., H., Abel, T., 2005, ApJ, 629, 615W
Wyithe, J.S.B., Loeb, A., 2003, ApJ, 590, 691
Wyithe, J.S.B., Loeb, A., 2005, ApJ, 634, 910W

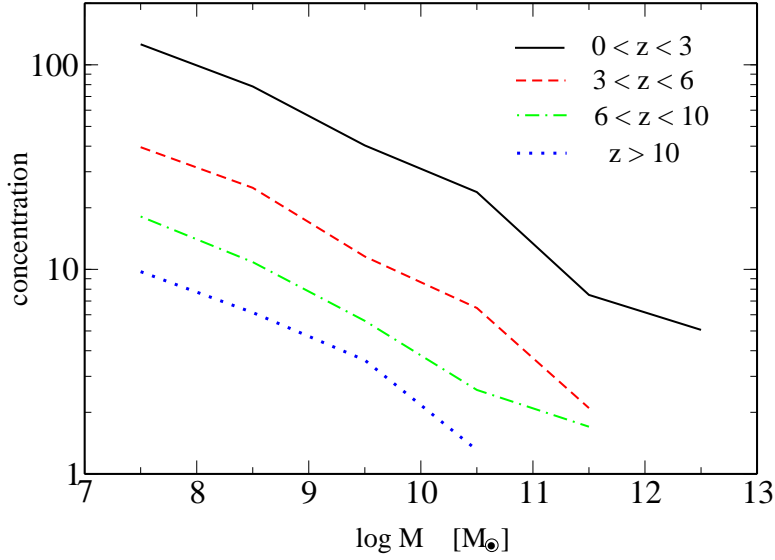


Figure 1. Average concentration parameter in four redshift ranges for all dark matter halos in our simulation as a function of halo mass.

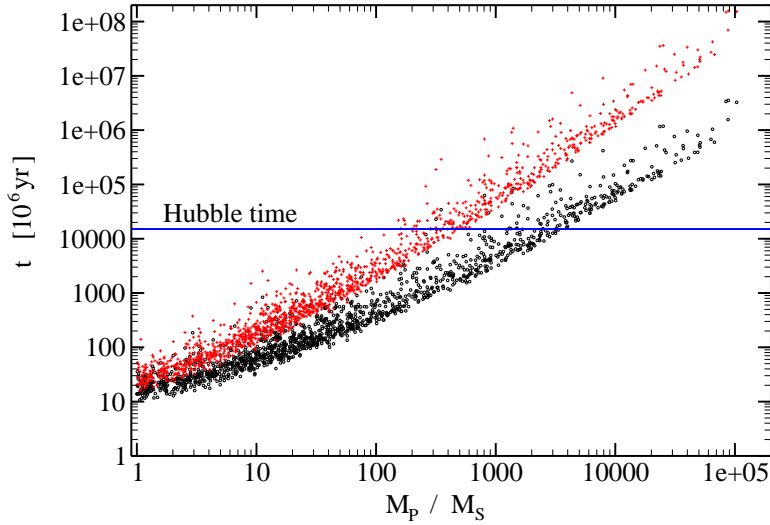


Figure 2. Time for each satellite to reach the primary halo center as a function of the mass ratio of merging halos. Black circles represent the Chandrasekhar dynamical friction time and red pluses represent the merging time calculated from a simulation-based numerical fit (Boylan-Kolchin 2008). Both timescales are compared to the Hubble time. Merging halos above the horizontal blue line will not finish their merger and are removed from the merger tree, but their positions are updated within the primary halo.

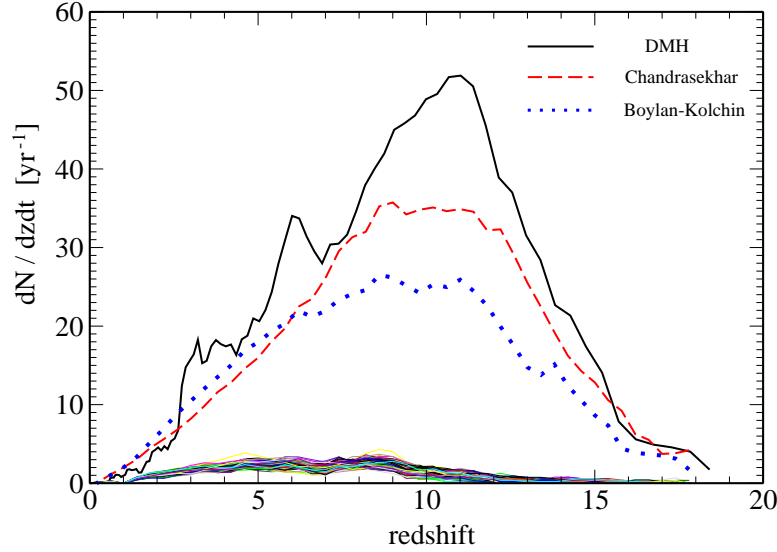


Figure 3. Top line (black): Black hole merger rates without dynamical friction. Note that in this case, this is equivalent to the dark matter halo merger rate; Dashed (red): Black hole merger rate with the Chandrasekhar dynamical friction formula; Dotted (blue): Black hole merger rate obtained from the Boylan-Kolchin numerical fit for dynamical friction. We predict that LISA black hole merger rates at $z \leq 2.7$ are larger than estimated by models based on Chandrasekhar dynamical friction. Bottom: 100 realizations of black hole merger rates for an initial seed black hole occupation fraction of 0.1, with Boylan-Kolchin dynamical friction. The maximum black hole merger rate of 3 is considered a pessimistic scenario.

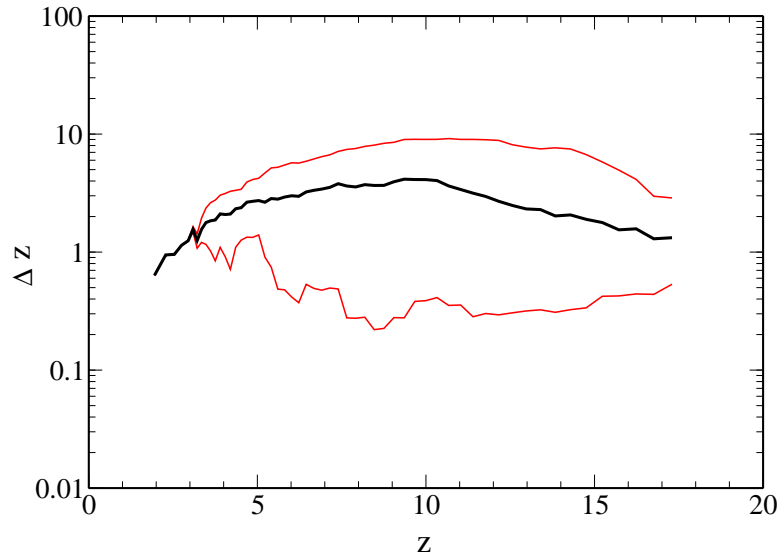


Figure 4. Thick black - average change in the merger redshift when dynamical friction is applied as a function of merger redshift (without dynamical friction). Red lines represent minimum and maximum shift in the redshift of black hole merger. Dynamical friction postpones black hole mergers toward lower redshifts, making them louder LISA sources and increasing the local rate as well.

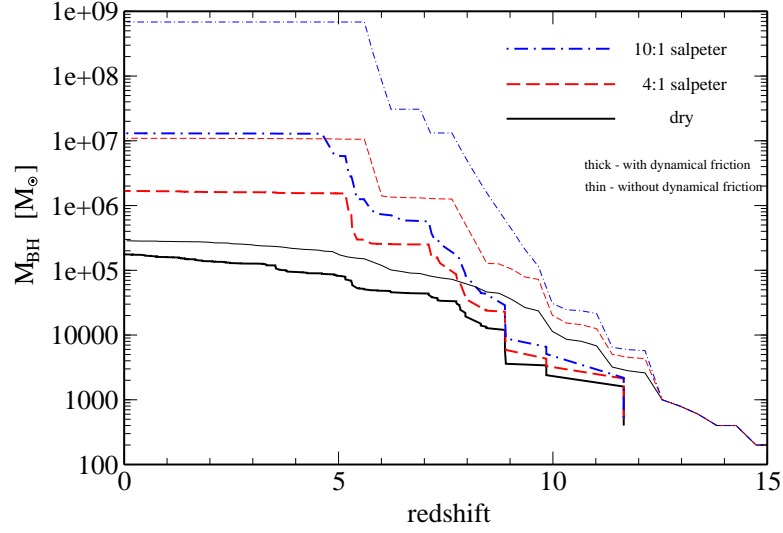


Figure 5. Mass of the central SMBH as a function of redshift. Thin lines correspond to SMBH growth using the prescription described in the text when dynamical friction is neglected. Thick lines represent SMBH growth with dynamical friction. “Dry” growth is in black; “4:1” growth in red; and “10:1” growth in blue. The final episode of gas accretion onto the SMBH is at redshift $z=4.7$ in the 10:1 case with dynamical friction. Later on, the SMBH grows through mergers only and its mass remains almost constant until $z=0$.

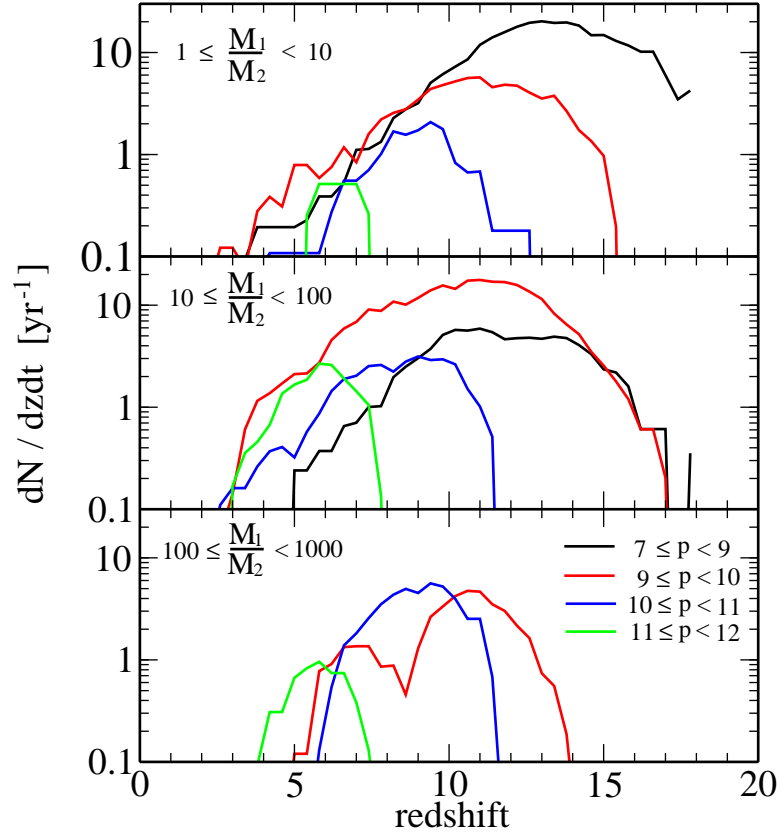


Figure 6. Dark matter halo merger rates as a function of redshift for all halos that finish merging by redshift zero. Three panels show various ranges for the halo mass ratio and the total combined halo mass. M_1 is mass of the primary halo, M_2 is mass of the satellite, and the total mass is defined by $p = \log(M_1 + M_2)$. The panel with $M_1/M_2 \leq 10$ shows merger rates for major mergers that activate gas accretion onto their black holes.

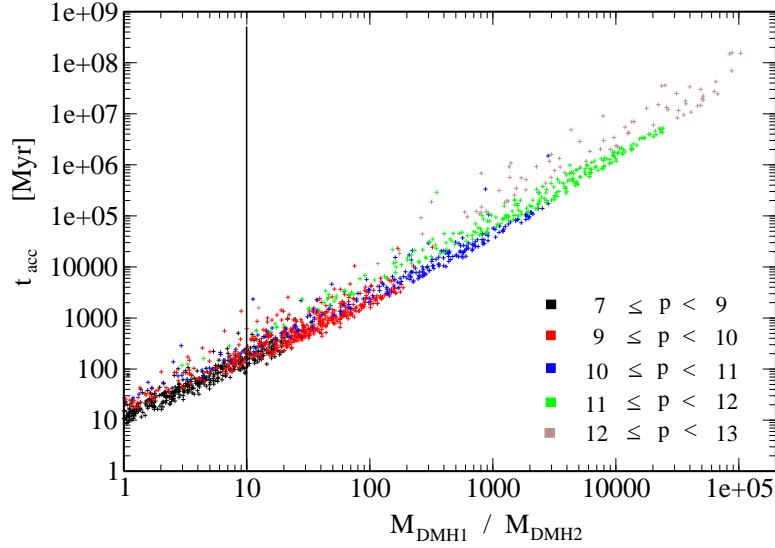


Figure 7. Gas accretion time, t_{acc} , for black holes at the center of a satellite halo of mass M_{DMH1} that is merging with a primary halo of mass M_{DMH2} . The total mass is denoted by $p = \log(M_{\text{DMH1}} + M_{\text{DMH2}})$, and $t_{\text{acc}} = t_{\text{merger}} - t_{\text{dyn}}$ where t_{merger} is the merger time scale, and t_{dyn} is the dynamical time, making accretion begin at the first pericenter pass. Only merging halos with mass ratio less than 10 (vertical line) will allow gas accretion onto the black holes.

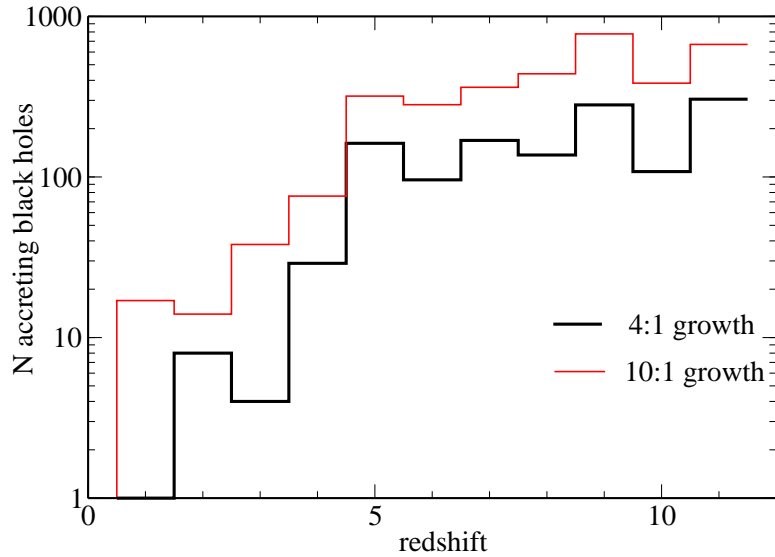


Figure 8. Number of accreting black holes as a function of redshift. Here we include both black holes that do and do not eventually merge. The rapid drop in the number of accreting black holes (for both 4:1 and 10:1 Salpeter growth) at redshift $z \sim 5$ corresponds to the end of SMBH growth at the primary halo center (Figure 4). The remaining black holes at low redshift correspond to black holes that are still sinking into the center by redshift zero.

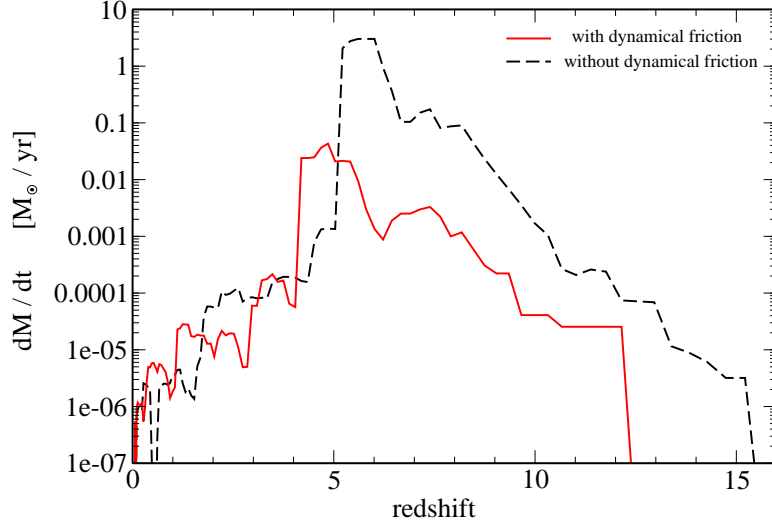


Figure 9. Mass growth rate of the SMBH as a function of redshift. Black dashed: “10:1” growth without dynamical friction. Red thick: “10:1” growth with dynamical friction. The SMBH growth is largely complete by redshift 4.7, as the merger-driven gas supply is depleted.

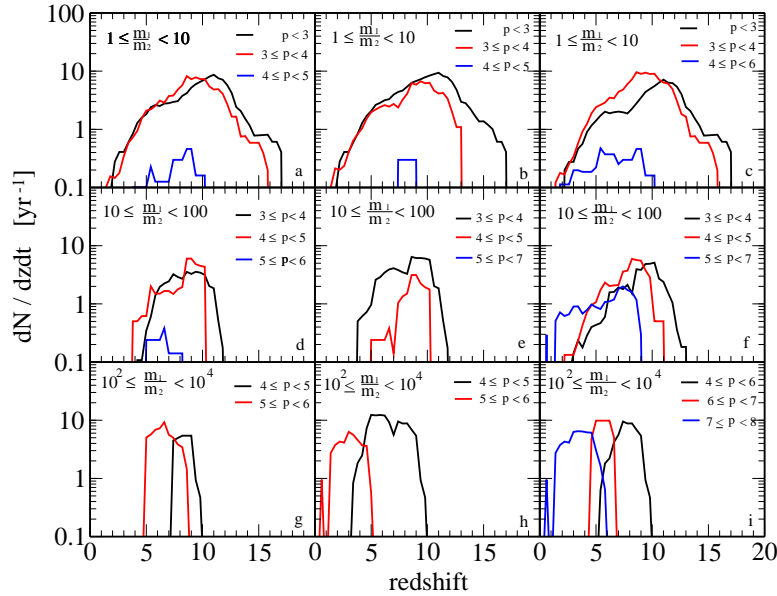


Figure 10. Black hole merger rates as a function of redshift for different binary mass ratios and total binary mass ranges, $p = \log(m_1 + m_2)$. Horizontally, we separate the merger rate by mass ratio: in panels a, b, and c, we focus on $1 \lesssim m_1/m_2 < 10$; $10 \lesssim m_1/m_2 < 100$ in d, e, f; and $10^2 \lesssim m_1/m_2 < 10000$ in g, h, i. Each column represents a different black hole growth scenario: we cover dry growth in a, d, g; 4:1 growth in b, e, h; and 10:1 growth in c, f, i. For redshifts $z \sim 1 - 5$ and mass ratios of $100 \lesssim m_1/m_2 < 10000$, the merger rate is 3 - 7 yr^{-1} in 4:1 case (h) and 10:1 case (i). These black hole mergers are in the appropriate mass and redshift range to be important LISA sources.

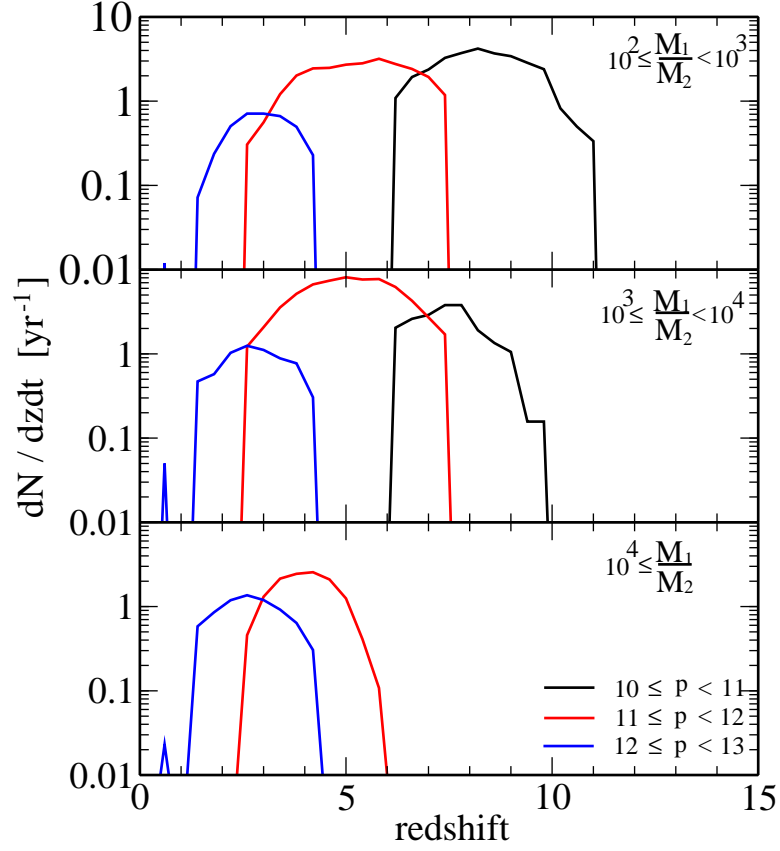


Figure 11. Rate that the primary captures rogue black holes. Most of the seed black holes were captured before redshift 5 and were hosted by low mass halos.

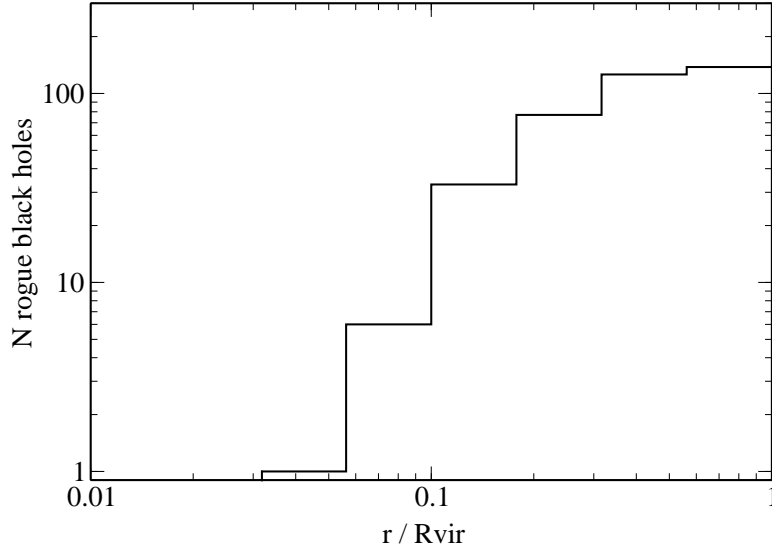


Figure 12. Distribution of massive rogue black holes inside the primary halo at redshift zero. The dark matter hosts of these rogue black holes have merged with the primary halo but the dynamical friction time is longer than the Hubble time. Hence, these massive black holes do not sink to the center by $z=0$.

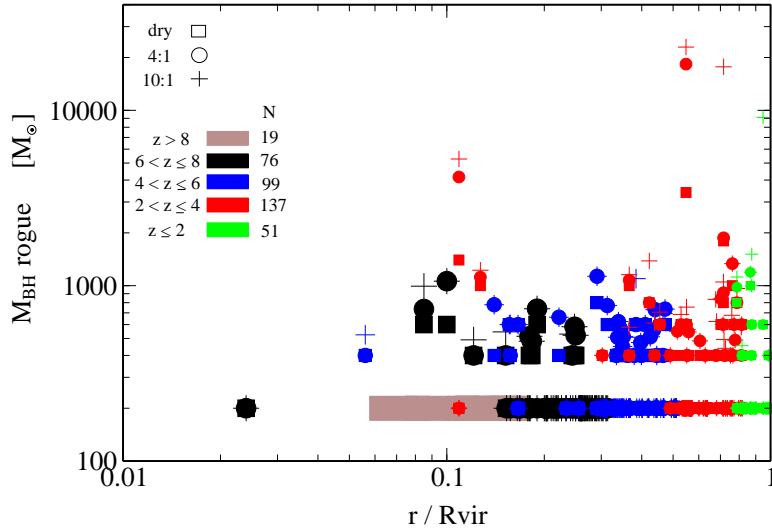


Figure 13. Rogue black hole mass as a function of virial radius for three accretion models with dynamical friction: “dry” in squares; “4:1” in circles; and “10:1” in pluses. Colors correspond to the redshift range where black hole became rogue – this is also the merger redshift of merger the primary and satellite halos. Many of the most massive rogue black holes are accreted late and have been ‘pre-processed’ with previous mergers of their own.

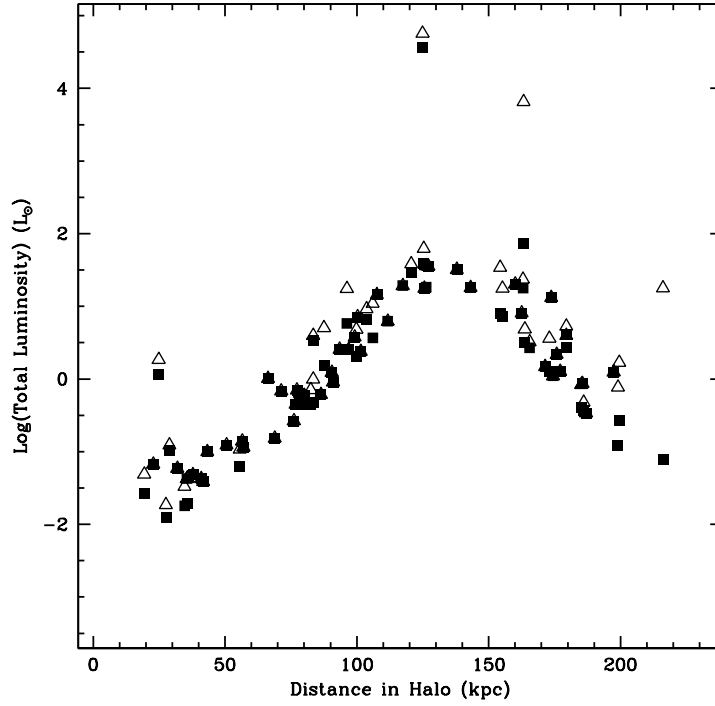


Figure 14. Bolometric luminosity of rogue black holes as a function of distance from the primary halo center. Black holes are assumed to accrete via a Bondi-Hoyle mechanism from the ambient gas in the primary. Blue squares represent our 10:1 accretion scenario, and red squares represent the 4:1 scenario. Most black holes will have roughly solar luminosities, but a few are expected to be luminous X-ray sources (just under the ULX cut-off) that reside in the Milky Way halo.

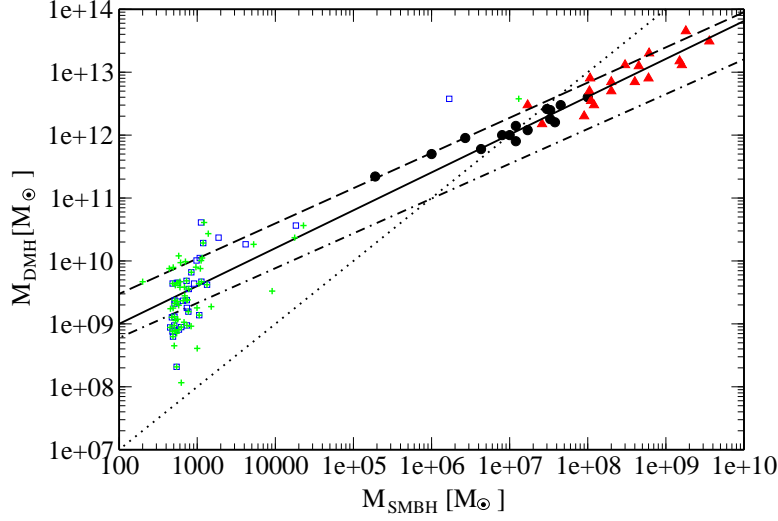


Figure 15. Dark matter halo mass as a function of central SMBH mass for spiral galaxies (filled circles) and elliptical galaxies (filled triangles) (data taken from Ferrarese 2002). The dotted line represents $M_{\text{DMH}} / M_{\text{BH}} = 10^5$. The solid line obtains a halo mass using Bullock et al. 2001 prescription to relate the virial velocity, v_{vir} , to the circular velocity, v_c . The dashed line shows the same function when $v_{\text{vir}} = v_c$, and the dot dashed line is for $v_c / v_{\text{vir}} = 1.8$ (Seljak 2002). Our results are presented as squares for the 4:1 black hole growth scenario and pluses for 10:1 growth scenario only for those black holes that have completed the merger by redshift zero. The primary halo and its central SMBH fit the M_{DMH} vs. M_{BH} relation for 10:1 growth scenario while satellites and their central black hole broadly fit the extrapolated M_{DMH} vs. M_{BH} relation.

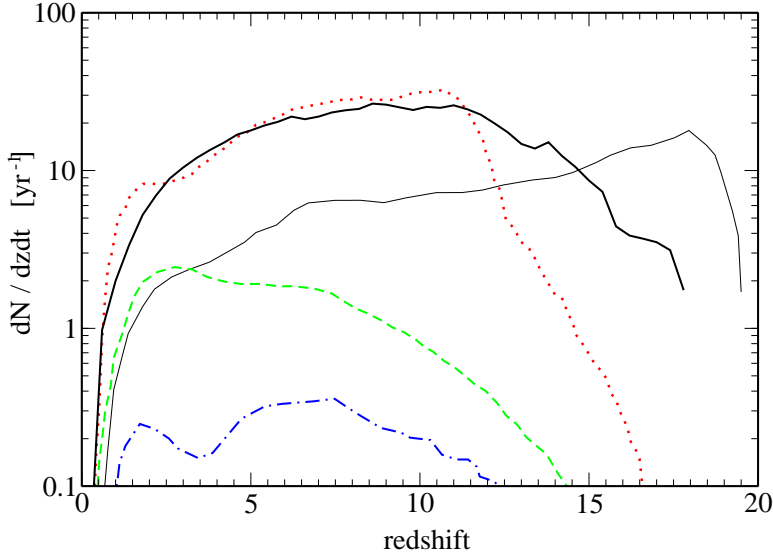


Figure 16. Merger rates observed at $z=0$ as a function of redshift for four models described in Sesana et al. 2007, all with a Chandrasekhar prescription for dynamical friction. The thin black line corresponds to massive DMHs ($M_{\text{DMH}} = 10^{11} - 10^{15} M_{\odot}$) seeded with $m_{\text{BH}} \sim 200 M_{\odot}$ black holes at $z=20$; The dot-red line represents low mass halos ($M_{\text{DMH}} = 10^6 - 10^7 M_{\odot}$) seeded with $m_{\text{BH}} \sim 5 \times 10^4 M_{\odot}$ at $15 \lesssim z \lesssim 20$; The blue-dashed line and black-dot line explore different redshift ranges for seeding black holes in halos: green: $m_{\text{BH}} = 10^4 - 10^5 M_{\odot}$ at $15 \lesssim z \lesssim 20$ and blue $18 \lesssim z \lesssim 20$. Overplotted in the thick black is the black hole merger rate when dynamical friction is modeled with an n-body based estimate of the dynamical friction decay time (Boylan-Kolchin et al. 2008)